E-ISSN 2586-9027
Homepage : https://tci-thaijo.org/index.php/SciTechAsia Science & Technology Asia
Vol.31 No.1 January - March 2026 Page: [314-326]
Original research article

Comparative Analysis of V-Shaped Rib Configurations for Enhanced Cooling Performance in Gas Turbine Blades

Kumpanat Chaiphet, Nattadon Pannucharoenwong*, Phadungsak Ratanadecho

Department of Mechanical Engineering, Faculty of Engineering,
Thammasat School of Engineering, Thammasat University, Pathum Thani 12120, Thailand

Received 29 July 2025; Received in revised form 4 December 2025
Accepted 7 January 2026; Available online 27 March 2026

ABSTRACT

This study conducts a numerical analysis of six different V-shaped rib configurations installed in a square internal cooling passage (aspect ratio, AR=1:1), representing a typical gas turbine blade cooling channel. Using the RNG $k-\varepsilon$ turbulence model, simulations were conducted for Re ranging from 5,000 - 30,000 to evaluate heat transfer and flow characteristics through three primary metrics: the Nusselt number (Nu), friction factor (f), and thermal enhancement factor (TEF). As Re increases, secondary vortices intensify, enhancing mixing and heat transfer. Although continuous V-shaped ribs (Model 1) provide the greatest heat transfer rate, they generate considerable flow resistance. Alternating continuous ribs (Model 2) achieve the highest TEF, particularly at lower Reynolds numbers, by balancing heat transfer improvement with moderate pressure losses. Discontinuous and alternating rib designs (Models 3–6) effectively decrease the pressure drop while sustaining acceptable heat transfer levels. These findings emphasize the importance of rib geometry in controlling turbulence, pressure loss, and thermal performance, offering valuable guidelines for optimizing internal cooling designs in turbine blades.

Keywords: Cooling passage; Gas turbine cooling; Thermal enhancement factor; Rib configurations; V-shaped ribs

1. Introduction

Gas turbines serve an essential function in the realms of energy generation and propulsion; however, their constituent elements—most notably the blades—are perpetually subjected to extreme thermal conditions. As a result, achieving effective internal cooling is essential. Among

***Corresponding author:** pnattado@engr.tu.ac.th **doi:** xx.xxxxx/scitechasia.xxxx.xx

the various cooling strategies, embedding V-shaped ribs within internal passages has been shown to markedly improve convective heat transfer by breaking up boundary layers and stirring the flow [1, 2].

Researchers have explored diverse rib designs to enhance performance. For instance, Wang et al. introduced interrupted V-shaped ribs that strategically disrupt flow, significantly boosting local cooling efficiency [1]. Pandya and Ekkad found that broken V ribs offer particularly strong heat transfer performance under high-Reynolds-number conditions [2]. Pathak and Kumar's work on combined V-rib–dimple geometries achieved a harmonious balance of enhanced cooling with moderate pressure loss [3]. Tamang et al. then designed a new rib shape suited for square ducts, achieving TEF ≈ 2.05 and highlighting its applicability in compact flow passages [4]. Continuing this trend, Say et al. developed Vspline ribs that deliver uniform heat transfer improvements [5]. Su and Liu's research comparison of shaped ribs in trapezoidal channels favored the V rib design, recording TEF ≈ 2.18 [6]. Narrower passage designs, including work by Krishnaswamy et al., confirmed that both V and Wribs effectively improve cooling in high aspect-ratio channels [7], while Matsuura et al. showed that side-wall ribs significantly shape boundary behavior and lift TEF to ≈ 2.22 [8]. Numerical and experimental investigations by Kamat's group reaffirmed the superiority of V-rib pavement, with TEFs ranging from ≈ 2.08 to 2.12 across conditions [9,10]. Leveraging CFD and AI-based genetic algorithms, Damavandi et al. achieved high-performing asymmetric V-rib configurations [11], which Kumar and Amano then validated experimentally using brokenV ribs [12].

In the context of rotating passages, studies showed W-shaped ribs as superior performers in balancing thermal and hydraulic efficiency [13]. Guo et al. revealed that dual-path U-channel designs with V-ribs drive efficient vortex structures that elevate heat transfer [14], and Chen et al. explored the effects of profiled V-ribs under rotation [15]. Computational analyses of modified V-rib layouts also proved effective in mitigating dead zones and enhancing TEF by ≈ 2.09 [16].

In more complex routes, Yoon et al. identified that alternating rib placements in serpentine channels notably improves thermal performance [17], while Thirumalai and Ekkad demonstrated that 45° broken V-ribs under rotation sustain high efficiency [18]. Real-world blade studies highlighted the importance of outlet geometry on cooling effectiveness [19], and Shi et al. concluded that combining dimple and protrusion features yields the best thermal advantage yet recorded [20].

Despite significant advances in rib design, a comprehensive comparison of different V-shaped rib geometries under identical boundary conditions remains lacking. To address this gap, the present study conducts numerical simulations using computational fluid dynamics (CFD) to evaluate six V-rib configurations including of continuous, alternating, truncated, and discrete within a rectangular channel with aspect ratio AR of 1:1. Key performance metrics, including Nusselt number (Nu), friction factor (f), and thermal enhancement factor (TEF), are assessed across a Reynolds number range of 5,000 to 30,000, with the goal of identifying optimal rib geometries for enhanced thermal performance in gas turbine cooling applications.

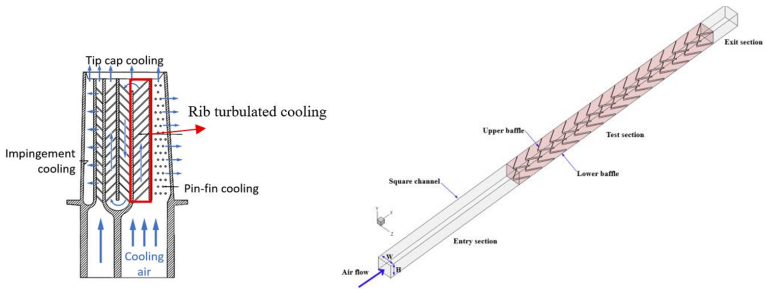

Fig. 1. (a) Illustration showing internal cooling methods used in modern gas turbine blades, and (b) a close-up view of the cooling passage.

2. Geometry of Cooling Passages and V-shaped Baffles

The cooling passages had a rectangular cross-section. V-type baffles were arranged on the heated surface on both the top and bottom walls, as illustrated in Fig. 1. The objective was to generate a primary vortex flow, in conjunction with a secondary motion that exhibits characteristics akin to those of an impinging jet. This flow interaction helped enhance thermal transfer due to minimized pressure losses alongside increased thermal exchange efficiency introduced via different V-shaped arrangements inside the duct, as shown in Fig. 2. The constructed channel was a single-pass rectangular duct characterized by dimensions of width (W) and height (H) each measuring 30 mm, leading to an aspect ratio (AR) of 1:1 and a hydraulic diameter (D_a) of 30 mm. The parameters of the baffle encompassed an angle of attack (α), a pitch ratio (PR = p/H), and a blockage ratio (BR = b/H), which were established at 30°, 1.0, and 0.1, respectively. The groove length (e/H) in each configuration was also specified. The turbulent flow regime was examined across a range of Reynolds numbers spanning from 5,000 to 30,000.

3. Boundary Conditions

The computational domain and mesh setup are illustrated in Fig. 3. Air was employed as the working medium, with its thermophysical properties evaluated at 300K as detailed in Table 1. A nonslip condition was imposed on all walls. A constant heat flux of 600 W/m^2 was imposed on both the upper and lower walls. The side walls (left and right) were treated as adiabatic, and the heat conduction through these walls was considered negligible.

Table 1. Thermophysical properties of air as working fluid at 300 K [22].

Unit	Value
Prandtl number (Pr)	0.707
Density, ρ(kg/m^3)	1.1614
Specific heat, Cp (J/kg·K)	1007
Thermal conductivity, ka (W/m·K)	0.0263
Dynamic viscosity, μ(kg/m·s)	0.00001846

4. Governing Equations and Numerical Methodology

The simulation of turbulent flow and heat transfer was carried out by solving the governing equations, assuming a steady, three-dimensional, and incompressible flow field. In this model, heat transfer was limited to convection only, excluding conduction within the solid walls.

The governing equations were as follows:

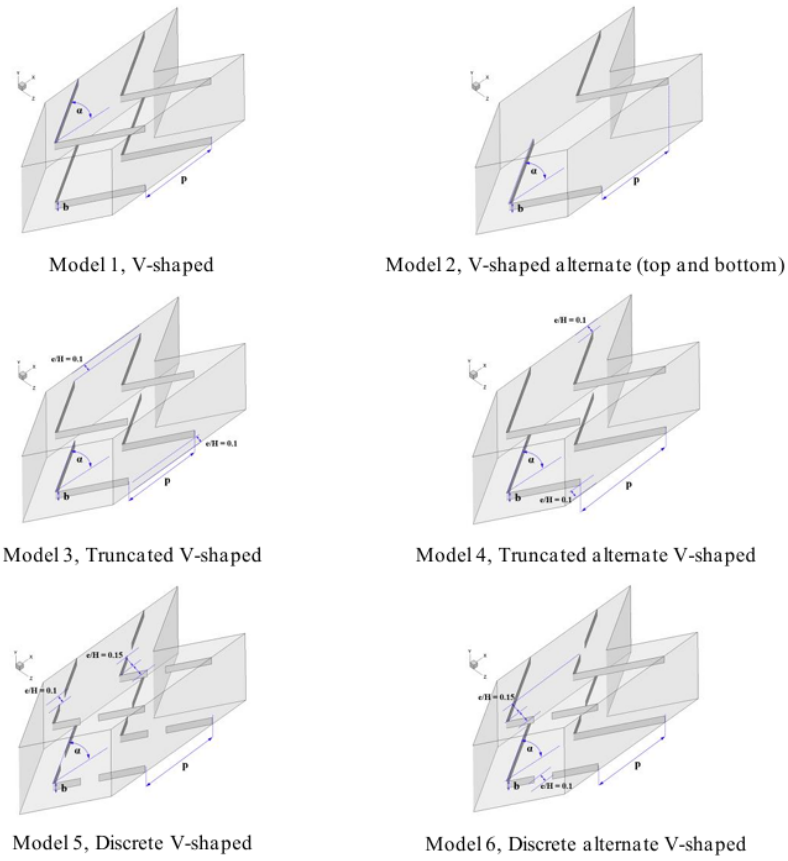

Fig. 2. Details of the various model V-shaped configuration.

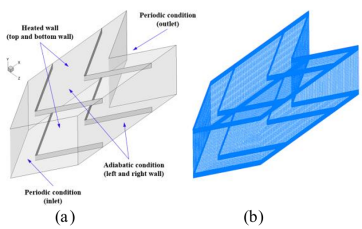

Fig. 3. (a) Geometry of the simulation domain and (b) generated mesh arrangement.

Continuity equation:

$$\frac{\partial}{\partial x_i}(\rho u_i) = 0. \qquad (4.1)$$

Momentum equation:

$$\frac{\partial}{\partial x_j}(\rho u_i u_j) = -\frac{\partial p}{\partial x_i} + \frac{\partial}{\partial x_j} \times \left[\mu\left(\frac{\partial u_i}{\partial x_j} - \rho\overline{u_i' u_j'}\right)\right]. \qquad (4.2)$$

Equation of Energy:

$$\frac{\partial}{\partial x_i}(\rho u_i T) = \frac{\partial}{\partial x_j}\left(\left(\frac{\mu}{\mathrm{Pr}} - \frac{\mu_t}{\mathrm{Pr}_t}\right)\frac{\partial T}{\partial x_j}\right), \qquad (4.3)$$

where

$$\mu_t = \rho C_\mu k^2/\varepsilon \text{ and } k = 0.5\overline{u_i' u_j'}.$$

The RNG $k-\varepsilon$ turbulence model was utilized to address this problem and is described as follows:

$$\frac{\partial}{\partial x_i}(\rho k u_i) = \frac{\partial}{\partial x_j}\left(\sigma_k(\mu + \mu_t)\frac{\partial k}{\partial x_j}\right)$$

$$+G_k + \rho\varepsilon \quad \text{for } k, \tag{4.4}$$

and

$$\frac{\partial}{\partial x_i}(\rho\varepsilon u_i) = \frac{\partial}{\partial x_j}\left(\sigma_\varepsilon(\mu+\mu_t)\frac{\partial \varepsilon}{\partial x_j}\right) + C'_{1\varepsilon}\frac{\varepsilon}{k}G_k - C_{2\varepsilon}\rho\frac{\varepsilon^2}{k} \quad \text{for } \varepsilon, \tag{4.5}$$

where the $C'_{1\varepsilon}$ can be expressed as

$$C'_{1\varepsilon} = C_{1\varepsilon} - \frac{\eta(1-\eta/\eta_0)}{1+\lambda\eta^3}$$

where

$$\eta = (2{\cdot}E_{ij}{\cdot}E_{ij})^{1/2}\frac{k}{\varepsilon} \text{ and } E_{ij} = \frac{1}{2}\left(\frac{\partial u_i}{\partial x_j} + \frac{\partial u_j}{\partial x_i}\right).$$

The constant values were

$$C_\mu = 0.09, \sigma_\varepsilon = 1.3, \sigma_k = 1.0, C_{1\varepsilon} = 1.42,$$

$$C_{2\varepsilon} = 1.68, \eta_0 = 4.377, \lambda = 0.012.$$

The governing equations were discretized using the Finite Volume Method [24]. A convergence threshold of 10^{-9} was set for the energy equation, whereas 10^{-5} was used for the remaining equations. The key parameters of interest in this study are summarized as follows: The Reynolds number:

$$\mathrm{Re} = \rho\bar{u}D_h/\mu, \tag{4.6}$$

which $\bar{u}$ denotes the mean velocity The friction factor:

$$f = ((-dp/dx)D_h)/(\frac{1}{2}\rho\bar{u}^2). \tag{4.7}$$

The local Nusselt number:

$$Nu_x = h_x D_h/k_a. \tag{4.8}$$

The average Nusselt number:

$$Nu = \frac{1}{A}\int Nu_x dA. \tag{4.9}$$

The hydraulic diameter of duct, D_h is defined as

$$D_h = (2\times W\times H)/(W+H). \tag{4.10}$$

The thermal enhancement factor (TEF) was adopted as the key metric for performance evaluation [23, 25]

$$TEF = \left(\frac{Nu}{Nu_0}\right) \Big/ \left(\frac{f}{f_0}\right)^{\frac{16}{55}}_{\mathrm{Re}}. \tag{4.11}$$

Nu_0 and f_0 were the values of the smooth rectangular duct only.

5. Results and Discussion

5.1 Validation of the numerical model

A comparative analysis of the Nusselt number (Nu) and friction factor (f) for a smooth channel was carried out using different turbulence models. These included the $k-\omega$ models (Standard and SST) and $k-\varepsilon$ variants (Standard, Realizable, and RNG), with results benchmarked against experimental data [21] and established correlations [22, 25], as illustrated in Fig. 4.

The simulation results showed that the variations of the Nusselt number (Nu) and friction factor (f) were consistent with the values predicted by empirical correlations and supported by experimental data. Among the evaluated models, the RNG-based $k-\varepsilon$ turbulence model yielded Nu and f values closely aligned with the reference data, with discrepancies within ±7%.

5.2 Grid independence

The effect of mesh resolution was examined using Model 1 with parameters BR = 0.1, P_R = 1.0, = 30° and Reynolds number of 5000. Seven different grids of 120,000, 260,000, 380,000, 510,000, 620,000, 730,000 and 850,000 were investigated at the same situation. Results indicated that increasing the grid count from

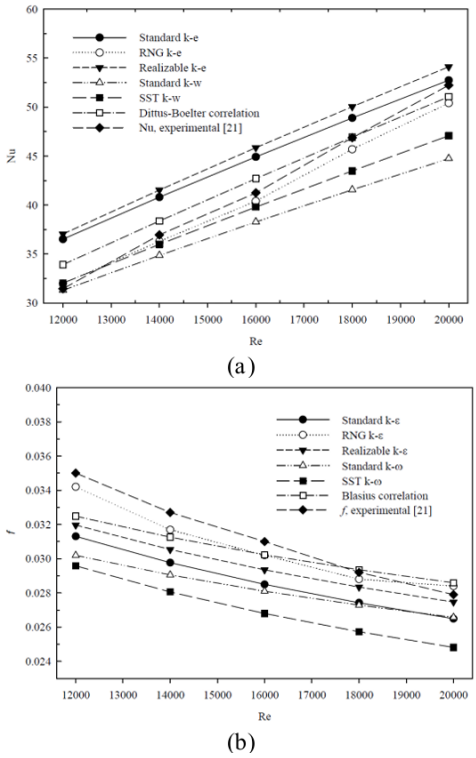

Fig. 4. Profiles of (a) Nusselt number and (b) friction factor along the flow.

730,000 to 850,000 caused a deviation in Nusselt number and friction factor of less than 0.5%. Considering both solution accuracy and computational time, the mesh size of 730,000 was selected for use in all simulations.

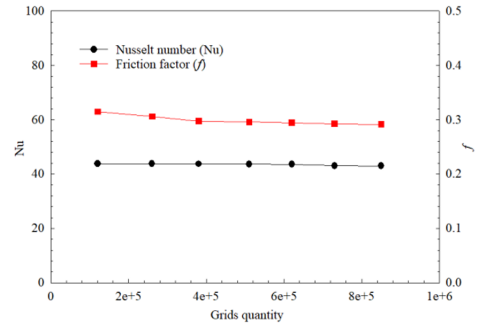

Fig. 5. Grid independent study for cooling passages.

5.3 Flow development and heat transfer characteristics

The velocity distributions inside the rectangular channel, illustrating the impact of baffle arrangements, are shown in Fig. 6. These profiles were obtained at the mid span positions of y/H = 0.5 and z/H = 0.5 for every case. In general, the flow behavior can be separated into two regions: the entrance zone and the fully developed periodic section. The V-shaped ribs accelerate the airflow due to the reduction of the flow cross-sectional area. For all cases, the flow reached a fully developed condition around x/H = 19. Similarly, the fully developed heat transfer data were collected at y/H = 0 and z/H = 0.5 for every model, with the profiles becoming periodic at approximately x/H = 18. The distribution of fully developed heat transfer oefficients (Nu/Nu_0) was found to closely follow the same trend as the velocity profiles, as displayed in Fig. 7.

5.4 Turbulent kinetic energy field and 2D local Nusselt number

Turbulent kinetic energy (TKE) contours in cross-sectional planes for Model 1 at different Reynolds numbers are shown in Fig. 8. As the Reynolds number increases, the vortex strength intensifies, indicated by the broader and denser TKE regions adjacent to the rib surfaces, reflecting stronger mixing and higher turbulence levels.

Comparison of TKE contours at Re=5000 for different V-shaped rib configurations is presented in Fig. 9. The results reveal that discrete and truncated ribs tend to generate stronger secondary flows and higher localized turbulence near the wall compared to continuous rib patterns, influencing heat transfer performance.

Fig. 10 shows local Nusselt number (Nu) contours at Re = 5000 for different V-shaped rib configurations. The heat

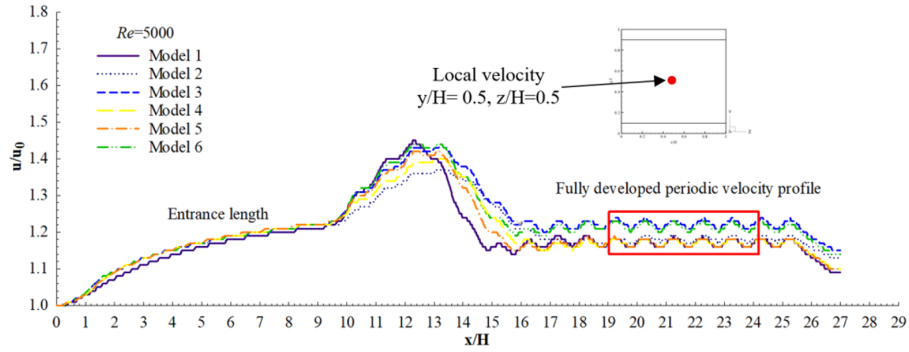

Fig. 6. Variation of u/u_0 along the channel for the various rib configurations.

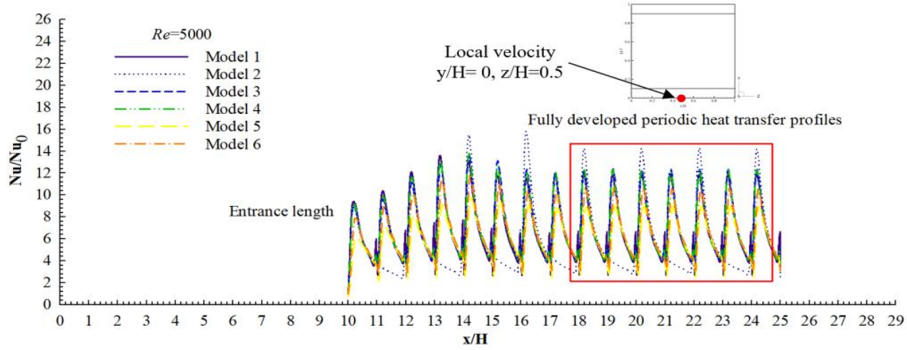

Fig. 7. Variation of Nu/Nu_0 along the channel for the various rib configurations.

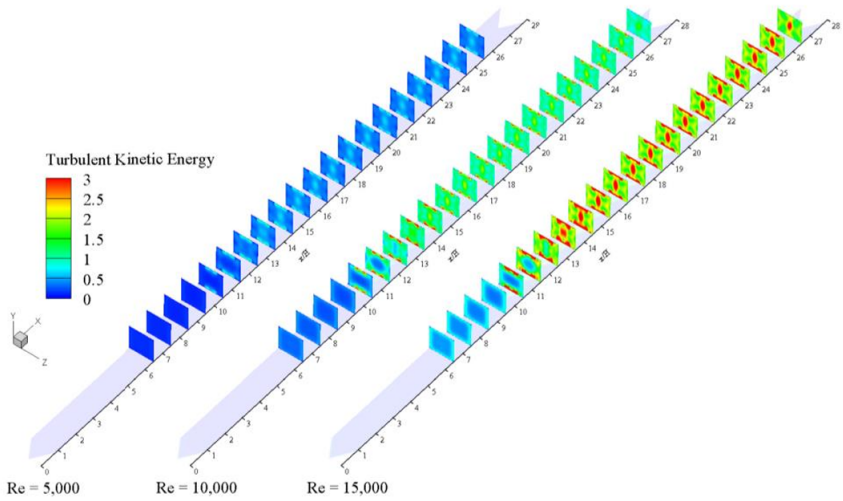

Fig. 8. Distribution of turbulent kinetic energy (TKE) across multiple cross-sectional planes in Model 1 at Re = 5,000, 10,000, and 15,000.

transfer distribution along the cooling channel bottom walls. The truncated and discretized ribs (models 3–6) show higher Nu concentrations near rib tips and downstream

regions, indicating stronger thermal boundary layer disruption. V-shaped ribs (models 1–2) yield more uniform but slightly lower Nu patterns. Alternating configurations produce asymmetrical contours, suggesting improved mixing. The results highlight the influence of rib geometry on local heat transfer enhancement.

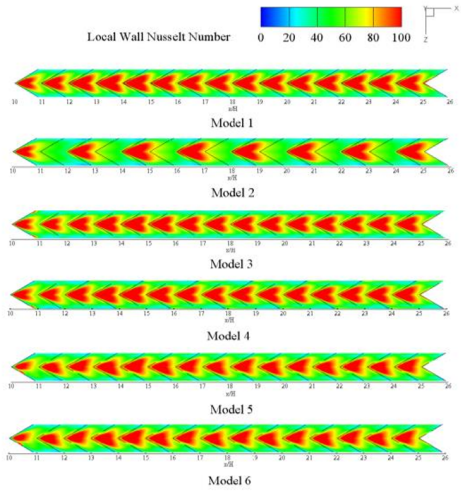

Fig. 9. The influence of local Nusselt number contour of Re=5000.

5.5 Comprehensive Assessment of Thermal–Hydraulic Performance

5.5.1 Analysis of heat transfer characteristics

Fig. 11(a) demonstrates that the average local wall Nusselt number increases consistently with the rise of Re for all rib configurations. This behavior reflects the enhanced convective transport that accompanies fully developed turbulent flow within internal cooling passages. Among the studied models, Model 1 exhibits the highest Nu across the entire Reynolds number range. Model 2 and Model 4 also show competitive heat transfer performance, particularly in the low to moderate Reynolds number regime (below 15,000). Models 5 and 6, which employ discontinuous and alternating rib arrangements, produce slightly lower Nu values but still provide significant heat transfer augmentation.

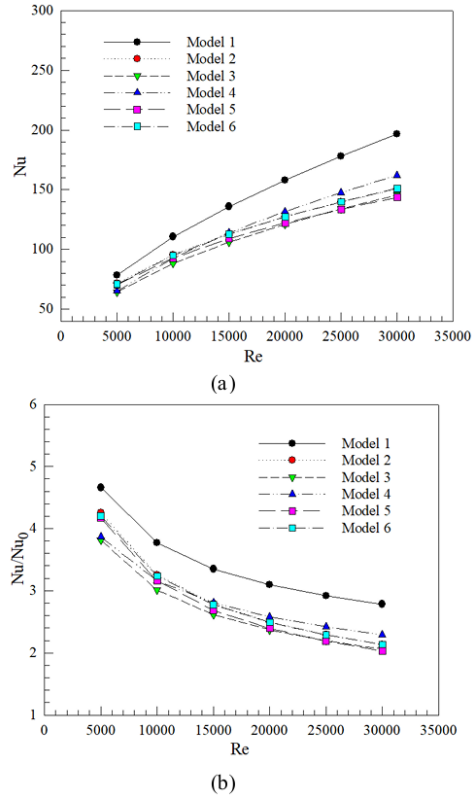

Fig. 10. The variations of (a) Nu and (b) Nu/Nu_0 various Re.

The distribution of the normalized Nusselt number (Nu/Nu_0) relative to a smooth duct is depicted in Fig. 11(b). A downward trend of Nu/Nu□ is evident as the Reynolds number increases. At Reynolds numbers below 10,000, several rib configurations achieve Nu/Nu□ values above 3.0, underscoring the effectiveness of rib-induced turbulence in promoting convective heat transfer under low to moderate flow conditions. As Re increases, however, the contribution of ribs to turbulence generation becomes progressively less dominant compared to inertial effects

in the flow, resulting in a gradual decrease of Nu/Nu_0 despite the continuing rise in absolute Nu. Comparative analysis shows that Model 2 maintains the highest Nu/Nu□ over most of the studied range, emphasizing its suitability for thermal enhancement in low and moderate Re applications. In contrast, Model 6 displays a sharper decline in Nu/Nu_0 as Re grows, indicating a design better suited to flow regimes where Reynolds numbers remain relatively low.

5.5.2 Analysis of frictional characteristics

The relationship between the friction factor (f) and Reynolds number (Re) for all six rib configurations is shown in Fig. 12(a). Across every configuration, the value of f declines as Re increases, reflecting the decreasing relative influence of viscous effects when flow velocity becomes higher. Among the six models, the fully continuous rib pattern of Model 1 causes the greatest flow obstruction, resulting in the highest friction factor at all Reynolds numbers. In contrast, Model 3—with its discontinuous segmented ribs—consistently gives the lowest f values, confirming that the separated structure reduces resistance to the moving fluid. A similar behavior is observed in Fig. 12(b) when considering the normalized friction factor (f/f_0) relative to a smooth square channel: the ratio gradually decreases with increasing Re for all designs. From the data, Model 1 stands out with the largest f/f_0 (around 7.16 at Re = 5000 and still 6.38 at Re = 30,000), while Model 3 shows the smallest values (about 5.12 at Re = 5000 and 4.29 at Re = 30,000). These results indicate that rib geometry strongly influences internal flow resistance, where discontinuous and segmented patterns reduce the pressure drop yet maintain enough turbulence to assist heat transfer. This makes such designs attractive in applications where a balance between enhanced heat transfer and reduced flow resistance is required.

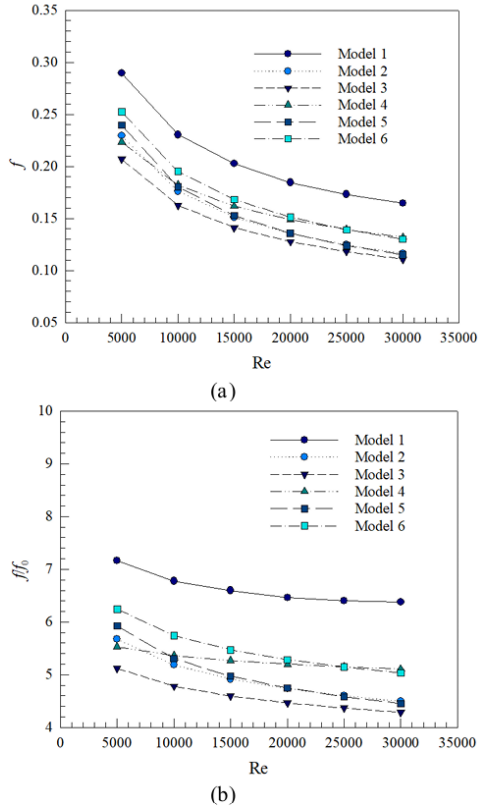

Fig. 11. Variations of (a) f and (b) f/f_0 various Re.

5.5.3 Thermal enhancement factor

Evaluation of Thermal Enhancement Factor (TEF) trends with Reynolds number for all rib configurations, Fig. 13, shows a consistent downward trend as the flow rate increases due to the dominance of inertial effects over turbulence-driven heat transfer at higher Reynolds numbers. At low Reynolds numbers (Re < 10,000), Model 1 demonstrates the highest TEF values, reaching approximately 2.4, which highlights its effective balance between heat transfer augmentation and the associated

pressure loss. Model 2 follows closely with values around 2.3, while Models 5 and 6, featuring discontinuous and alternating rib arrangements, provide TEF values in the range of 2.0–2.2, indicating good overall thermal performance with a moderate reduction in pressure drop. As the Reynolds number increases up to 30,000, TEF values for all models decrease gradually but remain above 1.2, confirming that these ribbed configurations maintain efficiency even in high-flow regimes. The data of calculated TEF values supports these observations, with Model 1 consistently achieving the highest TEF across the studied range, while Model 3, despite its low friction factor, yields slightly lower TEF due to reduced heat transfer performance. These results suggest that while continuous ribs can maximize thermal enhancement, rib designs incorporating discontinuities or alternating patterns are advantageous when the objective is to balance improved heat transfer with reduced flow resistance, making them suitable for a range of cooling applications.

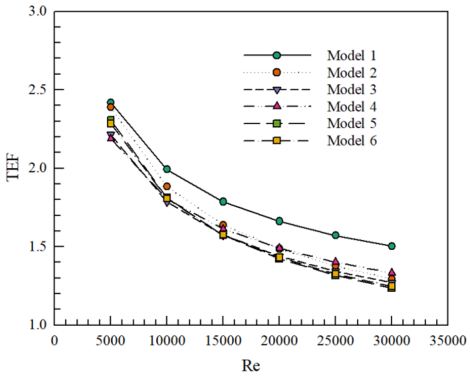

Fig. 12. Variation of TEF with Reynolds number for different rib configurations.

6. Conclusion

The six model of the single-pass rectangular channel is explicitly. The baffle has the attack angle (α), pitch ratio (PR = p/H), blockage ratios (BR = b/H) and aspect ratio (AR) were fixed at 30°, 1.0, 0.1 and 1:1, respectively. The turbulent flow regime was investigated on Reynold numbers in the range of 5,000 to 30,000, and the main findings were as follows:

1. Effect of Reynolds Number on Flow Behavior

Increasing the Reynolds number enhances turbulent kinetic energy, resulting in more intense and coherent vortex structures behind the ribs. This stronger turbulence improves fluid mixing and convective heat transfer, confirming the critical influence of Re on turbulence-driven transport in ribbed channels.

2. Effect of Rib Configurations on Local Turbulence and Heat Transfer

Rib geometry significantly shapes the flow structure. Discontinuous and alternating ribs (Models 3–6) create stronger localized turbulence than continuous ribs (Models 1–2). Asymmetric rib placement produces complex secondary flows, reduces recirculation zones, and raises local heat transfer, especially at rib edges.

3. Behavior of Nusselt number and Nu/Nu_0

Across all ribbed configurations, the average Nusselt number shows a consistent increase with the Reynolds number. At Re = 5,000, the updated normalized Nusselt number ratios (Nu/Nu_0) for Models 1 to 6 were 7.16, 5.67, 5.12, 5.53, 5.92, and 6.24, respectively. These results clearly indicate that Model 1 provides the highest Nu/Nu□ value in the low Reynolds number regime.

4. Friction Factor and Flow Resistance

Model 1 has the highest relative resistance, with f/f_0 = 4.66 at Re = 5,000, due to the fully continuous rib design. In contrast, Model 3 shows the lowest f/f_0 = 3.82, indicating better pressure-drop management while still sustaining turbulence levels.

5. Thermal Performance Factor (TEF)

The results show that the TEF values at Re = 5,000 were 2.42, 2.39, 2.21, 2.19, 2.31 and 2.28 for Model 1-6, respectively. Among these, Model 1 and Model 2 demonstrate slightly better thermal–hydraulic balance, while Models 3–6 also provide effective trade-offs between heat transfer and flow resistance. Despite TEF decreasing as Re rises, segmented and alternating ribs retain superior overall performance compared to continuous ribs.

6. Recommended Rib Configurations for Different Flow Regimes

Under different operating conditions, the optimal rib configuration depends on achieving a balance between heat transfer and pressure loss. Continuous V-shaped ribs (Model 1) are most effective at low Reynolds numbers but impose high friction. Alternating ribs (Model 2) provide a better thermal–hydraulic balance at moderate Reynolds numbers. At higher Reynolds numbers, discontinuous ribs (Models 3–6) become preferable due to their lower pressure drop, with Model 3 offering the lowest friction for applications where minimizing flow resistance is essential.

These findings guide optimal rib design for turbine blade cooling by balancing heat transfer and pressure loss. Future work should consider the integration of perforated ribs or ribs with internal holes to further manipulate flow structures and reduce pressure drop. Additionally, evaluating these rib configurations under rotating conditions would provide a more realistic assessment of their performance in actual turbine environments.

7. Acknowledgements

This research was financially supported by Graduate Studies Faculty of Engineering, Thammasat School of Engineering, Thammasat University.

References

[1] Wang K, An H, Zhang Z, Zhang Y, Wu Z. Impact of V-shaped interrupted ribs in cross-flow channels on film cooling. Thermal Science. 2024;00:135.

[2] Pandya NS, Ekkad SV. Advanced thermal performance of broken V-shaped ribs for gas turbine blade internal cooling at high Reynolds numbers. 2024. Available from: doi:10.2514/6.2024-2759.

[3] Pathak M, Kumar A. Flow and heat transfer characteristics of gas turbine blade channels with compound V-rib-dimple structures. 2024. Available from: doi:10.2139/ssrn.4834656.

[4] Tamang S, Ali E, Park H. A novel concept for a rib turbulator for optimizing the cooling performance in a square channel. Int J Heat Mass Transf. 2024;197:125144.

[5] Say SY, Singh AD, Chow WT. V-spline design for enhanced performance in turbine blade internal cooling. J Eng Gas Turbines Power. 2024;146(7):073001.

[6] Su WJ, Liu YH. Thermal performance of V-shaped and X-shaped ribs in trapezoidal cooling channels. Energies. 2021;14(16):4826.

[7] Krishnaswamy K, Sivan S, Ali HM. Influence of narrow rectangular channel (AR = 1:4) on heat transfer and friction for V- and W-shaped ribs in turbine blade applications. Int J Photoenergy. 2021;2021:5581081.

[8] Matsuura K, Yoshida T, Hata D, Miyabe M. Effect of side-wall ribs on heat transfer and flow characteristics in internal cooling passage of gas turbine blade. J Phys Conf Ser. 2022;2217(1):012057.

[9] Kamat H, Shenoy SB, Kini CR. Effect of V-shaped ribs on internal cooling of gas turbine blades. J Eng Technol Sci. 2017;49(4):520-33.

[10] Kamat H, Kamath RC. Numerical simulation of internal cooling effect of gas turbine blades using V-shaped ribs. 2017. Available from: https://eprints.manipal.edu/148600/.

[11] Damavandi MD, Safikhani H, Yahyaabadi M. Multi-objective optimization of asymmetric V-shaped ribs in a cooling channel using CFD, artificial neural networks and genetic algorithms. J Braz Soc Mech Sci Eng. 2017;39(6):2319-29.

[12] Kumar S, Amano RS. Experimental investigation of heat transfer and flow using V and broken V ribs within gas turbine blade cooling passage. Heat Mass Transf. 2015;51(5):631-47.

[13] Wright LM, Fu WL, Han JC. Thermal performance of angled, V-shaped, and W-shaped rib turbulators in rotating rectangular cooling channels (AR = 4:1). J Turbomach. 2004;126(4):604-14.

[14] Guo X, Li X, Wang J. Thermal and flow characteristics of a double-paths V-ribbed U channel. Phys Fluids. 2024;36(10).

[15] Chen IL, Lee YT, Wang CL, Tsai HW. Heat transfer in a rotating, two-pass, variable aspect ratio cooling channel with profiled V-shaped ribs. ASME Turbo Expo. 2020;143.

[16] Case studies on enhanced heat transfer in a square duct with modified V-shaped ribs (MVR): A CFD analysis. Modell Simul Eng. 2022;2022:5376486.

[17] Yoon C, Ellinger M, Bogard DG. Evaluation of pressure drop and cooling effectiveness of serpentine channels with varying internal rib configurations. ASME Turbo Expo. 2023. Available from: doi:10.1115/gt2023-104216.

[18] Thirumalai M, Ekkad SV. Effect of rotation on 45-degree broken V-ribs in a 2-pass square channel. ASME Turbo Expo. 2024. Available from: doi:10.1115/gt2024-128221.

[19] Louisiana State University. Turbine blade internal cooling: Trailing edge, coolant-passage entry, bend effect and improvement in thermal performance. 2022. Available from: doi:10.31390/gradschool_dissertations.1774.

[20] Shi D, Xu T, Chen Z, Zhang D, Xie Y. The effect of dimple/protrusion arrangements on the comprehensive thermal performance of variable cross-section rotating channels for gas turbine blades. Int J Therm Sci. 2024;197:108733.

[21] Gajghate SS, Deshpande OP, Desai AU, Deshmukh AD, Kharade SU, Pal S, Cardoso EM, Saha BB, Bhaumik S. Effect of ribs configurations on heat transfer enhancement for W-shaped ribs in a square duct. Arab J Sci Eng. 2023;48(9):12141–60.

[22] Incropera F, Dewitt PD. Introduction to Heat Transfer. 3rd ed. New York: John Wiley & Sons Inc.; 2006.

[23] Thianpong C, Promvonge P, Skullong S, Promthaisong P, Nakhchi ME. Numerical heat transfer study of square duct equipped with novel flapped V-baffles. Int J Therm Sci. 2024;197:108819.

[24] Patankar SV. Numerical Heat Transfer and Fluid Flow. New York: McGraw-Hill; 1980.

[25] Turakarn C, Promthaisong P, Chompookham T. Thermal performance enhancement in a solar air heater fitted with

flapped V-baffles: Numerical study. Case Stud Therm Eng. 2025;69:105995.

Appendix

Nomenclature

A	surface area, m^2
A_R	aspect ratio, (–)
B_R	blockage ratio, (–)
b	baffle height, m
$C_{1\varepsilon}$	turbulence model coefficient, (–)
$C_{2\varepsilon}$	constant of the turbulence model,(–)
C_μ	mean strain and rotation rate function, (–)
C_p	specific heat, J kg^1 K^1
D_h	hydraulic diameter, m
E_{ij}	tensor of mean strain rate, s^1
f	friction factor, (–)
G_k	turbulent kinetic energy production by mean velocity gradients, kg s^3 m^1
H	channel height, mm
h_x	coefficient of the local convective heat transfer, W $m^2 K^{–1}$
k	turbulence kinetic energy, m^2 s^2
k_a	air thermal conductivity, W m^1 K^1
Nu	average Nusselt number, (–)
Nu_x	local wall Nusselt number, (–)
p	static pressure, Pa
P_R	pitch ratio, (–)
Pr	Prandtl number, (–)
P	distance between baffles, m
Re	Reynolds number, (–)
TEF	thermal enhancement factor, (–)
T	temperature, K
u	air velocity, W ms^1
u_i	x_i–direction velocity component
u_i'	x_i–direction fluctuation velocity
u_j	x_j–direction velocity component
u_j'	x_j–direction fluctuation velocity
VG	vortex generator, (–)
W	channel width, mm
x_i, x_j	coordinate direction, m

Greek letters

α	attack angle, degree
ρ	density, kg m^3
δ_{ij}	Kronecker delta, m
σ_k	turbulent Prandtl numbers, (–)
σ_ε	turbulent Prandtl numbers, (–)
η	ratio of turbulence mean strain, (–)
ε	rate of turbulent dissipation, m^2 s^3
μ	dynamic viscosity, kg m^1 s^1

Subscripts

0	smooth flat channel
a	air
t	turbulence
x	local

Superscripts

–	average